Understanding Heat Transfer Mechanisms in Recessed LED Luminaires

Tianming Dong and Nadarajah Narendran

Lighting Research Center
Rensselaer Polytechnic Institute, Troy, NY 12180
www.lrc.rpi.edu

Dong, T., and N. Narendran. 2009. Understanding heat transfer mechanisms in recessed LED luminaires. *Ninth International Conference on Solid State Lighting, August 3-5, 2009, San Diego, Proceedings of SPIE* 7422: 74220V.

Understanding heat transfer mechanisms in recessed LED luminaires

Tianming Dong and Nadarajah Narendran
Lighting Research Center, Rensselaer Polytechnic Institute, 21 Union St., Troy, NY, USA 12180

ABSTRACT

Reduced maintenance cost due to the long life of light-emitting diodes (LEDs) has attracted the lighting community to this rapidly evolving lighting technology. A high LED junction temperature negatively affects the performance of LEDs. To realize the long-life potential of LEDs, proper thermal management is necessary. This paper describes a numerical and experimental investigation of thermal solutions for an LED recessed downlight under passive cooling. Different heat transfer mechanisms and their contributions for keeping the LED junction at lower temperatures also were analyzed.

Keywords: light-emitting diode (LED), junction temperature, life, thermal management, heat transfer, passive cooling, natural convection, radiation.

1. INTRODUCTION

The promise of light-emitting diodes (LEDs) as energy-efficient and long-lasting light sources for general illumination has attracted attention from the lighting industry. LED fixtures for commercial and residential applications continue to emerge in the market. Although LEDs are commonly advertised to have a life of 50,000 to 100,000 hours, they could fail after only a few thousand hours when used in fixtures. The major problem is poor thermal management, which results in high LED junction temperature. The negative impact of LED junction temperature on LED life and optical performance has been shown in several studies.[1-3] Therefore, proper thermal management in LED fixtures is necessary to keep LEDs operating at appropriate junction temperatures and ensure long life and stable optical performance.

A number of thermal management techniques for high-power electronics, including LED systems, have been investigated at both the package level (e.g., reducing the thermal resistance of a single LED package) and the system level (e.g., increasing heat dissipation from the heat sink to the ambient by active or passive cooling).[4-7] For recessed LED fixtures under passive cooling, heat is conducted to a heat sink from the LED junction and then dissipated to the ambient by natural convection and radiation. When a recessed fixture is based on a specific LED package, heat sink performance determines the LED junction temperature. In literature, improvement of the convection heat transfer of heat sinks for passive cooling by using extended surfaces has been extensively investigated. Commonly used extended surfaces are plate fins and pin fins, which significantly increase the heat transfer area over unfinned heat sinks.[8-9] One study on recessed luminaires also showed that heat sink performance was affected by fin locations.[10] In addition, a novel heat sink design that utilizes the chimney effect induced by vertical tubes was proposed to enhance natural air flow for heat dissipation in high power electronics.[11] Apart from improved convection heat transfer in finned heat sinks due to an increased heat transfer area, past studies have shown that radiation heat transfer can account for a significant portion of total heat transfer under passive cooling.[12-13] By increasing surface emissivity, the contribution of radiation heat transfer was shown to be as much as 50 percent of the total heat transfer.[12-13]

In this study, thermal solutions for an LED recessed downlight under passive cooling (or natural convection) were investigated numerically and experimentally. Based on past literature, three thermal management concepts—pin and tube fins, extended surface area below the ceiling plane, and increased radiation by increased surface emissivity—were analyzed and compared. The goal was to lower the temperature of the heat sink where the LEDs were mounted at specified heat dissipation. First, numerical simulations were conducted on a scaled-down, 2.5 in. (63.5 mm) diameter, LED recessed downlight to analyze the contributions of the three heat transfer mechanisms—conduction, convection, and radiation—for cooling the heat sink. Then an experiment was carried out to validate the simulation results. Based on this initial study, a 4 in. (101.6 mm) diameter LED recessed fixture was designed and prototyped with optimized heat dissipation to keep the LED junction temperature low. The fixture was thermally tested to confirm the design feasibility. Additional numerical optimization was performed to study the effect of design parameters on heat sink temperature.

* Corresponding author e-mail: narenn2@rpi.edu; website: www.lrc.rpi.edu

2. PROBLEM DEFINITION

Figure 1a shows a schematic of the scaled-down downlight fixture, which was considered the base case for heat sink temperature comparison in this study. In this configuration, an aluminum can (height [H] = 2.5 in. [63.5 mm], diameter [D] = 2.5 in. [63.5 mm], wall thickness [t_w] = 0.125 in. [3.2 mm]) was recessed in an insulated ceiling, and inside the recessed can was mounted an LED recessed downlight fixture consisting of a flat round aluminum heat sink (2.5 in. [63.5 mm] diameter and 0.125 in. [3.2 mm] thickness) and a high-power LED. The front of the heat sink was exposed to the ambient air, and the back was enclosed by the recessed can. The fixture was cooled by natural convection, radiation, and conduction. In the figure, T_{bc} and T_a are boundary temperature and ambient temperature, respectively. In this study the boundaries were set equal to the ambient temperature (i.e., $T_{bc} = T_a$).

Figure 1b shows a one-dimensional thermal resistance model to illustrate the thermal paths for transferring heat generated by the LED in steady state. The figure shows three major heat transfer paths based on the assumption that the temperatures of the heat sink and the recessed can are the same and the temperature distributions are uniform. Also, the thermal path between the back of the heat sink and the recessed can was neglected because they have the same temperature as assumed above, and hence no heat flows through the path. In the thermal resistance network, $R_{\theta,j-b}$ is the thermal resistance of the LED package between junction and board, which is determined by the specific LED type; R_c is the contact thermal resistance between the LED board and heat sink, which is dependent on the attachment method; $R_{conv,hs-f}$ and $R_{rad,hs-f}$ are convective and radiative thermal resistances, respectively, between the front of the heat sink and the ambient, which is affected by the heat sink design; $R_{conv,can}$ and $R_{rad,can}$ are convective and radiative thermal resistances, respectively, between the exposed surfaces of the can and the ambient, which is also influenced by the heat sink design; $R_{cond,i}$ and $R_{cond,c}$ are the conduction thermal resistances of the insulation and ceiling, respectively, which are predetermined by the insulation and ceiling materials. Since only $R_{conv,hs-f}$, $R_{rad,hs-f}$, $R_{conv,can}$, and $R_{rad,can}$ (Figure 1b dashed rectangle) are affected by the heat sink design, in later analysis these thermal resistances are calculated according to the equations below to explain the contribution of different heat transfer mechanisms to each heat sink design.

$$R_{conv,hs-f} = \frac{T_{hs} - T_a}{Q_{1,conv}}, \qquad R_{rad,hs-f} = \frac{T_{hs} - T_a}{Q_{1,rad}}, \qquad R_{conv,can} = \frac{T_{hs} - T_a}{Q_{2,conv}}, \qquad R_{rad,can} = \frac{T_{hs} - T_a}{Q_{2,rad}}$$

In Figure 1b, T_j is the maximum LED junction temperature, T_b is the LED board temperature, T_{hs} is the maximum temperature of the heat sink, T_a is the ambient temperature, and T_{bc} is the temperature on the boundary of the insulation material and ceiling. In the experiment, T_{bc} is a controlled equal to T_a , and T_{hs} was measured and used to validate simulation results because T_j cannot be measured directly.

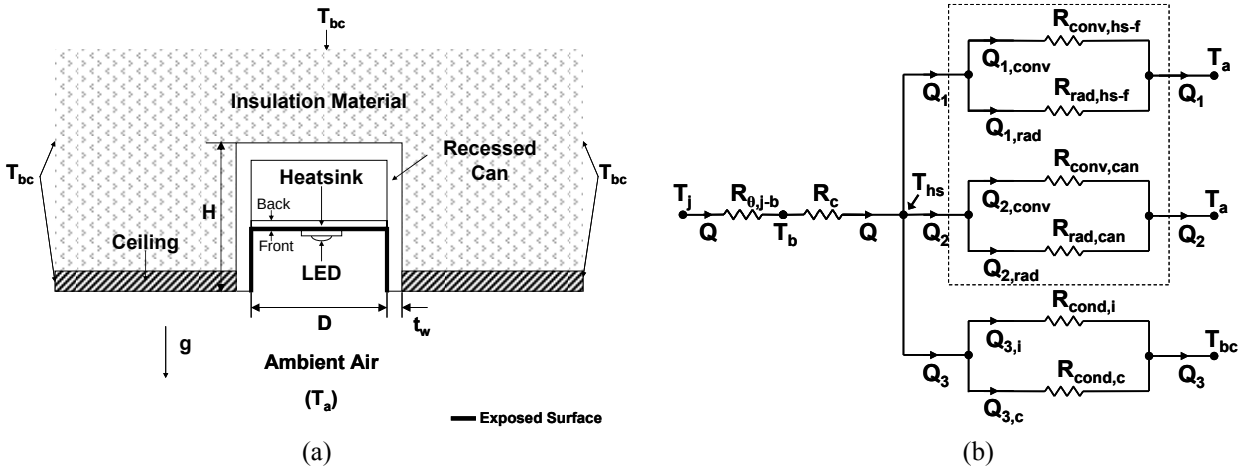

Fig. 1. (a) Schematic of the base case (b) One-dimensional thermal resistance network

3. EXPERIMENT

Figure 2 shows a schematic of the experiment apparatus, which consisted of a multidirectional fiber (MDF) board, three polystyrene foams, a plexiglass enclosure, and a foundation. In the center of the MDF board, a hole was cut for fitting the recessed can, as shown in Figure 1. Three sheets of polystyrene foam (each 2 in. [50.8 mm] thick) were used to insulate the recessed can and the back of the MDF board so that the setup maintained approximately room temperature on its boundaries. The plexiglass enclosure (35 in. × 23.5 in. × 25 in. [0.89 m × 0.60 m × 0.64 m]) was built to create a natural convection condition and prevent strays. T-type thermocouples (TC4 through TC14) were attached to the apparatus for temperature measurement. TC4 was glued using thermal epoxy to the top of the recessed can. TC5-TC8 were inserted in the MDF board, TC9-TC12 in polystyrene foam, and TC13 on the top of the polystyrene foam to evaluate conduction heat loss. TC14, shielded by a ceramic tube to prevent radiation heating, was attached to one of the plexiglass walls to monitor the ambient temperature inside the plexiglass enclosure. The locations of the thermocouples are shown in Figure 2 and Figure 3.

Four aluminum heat sink assemblies were made for experimentation and numerical model validation. Figure 4a shows an exploded view of a heat sink assembly and heat source attachment. Each heat sink was composed of a base plate and three tubes. The base plate had six holes (0.625 in. [15.9 mm] diameter) drilled along the periphery, three for press fitting the tubes. The other three served as outlets. In the center of the base plate, a round bump of 0.78 in. (19.8 mm) diameter and 0.06 in. (1.5 mm) thickness was machined to mimic the footprint of a typical high-power LED package. A resistive heater (Minco HK5572) with adhesive back was pasted on the bump and then covered by a thin piece of aluminum foil whose surface emissivity was measured. The resistive heater was used instead of an LED because of its convenience for specifying input heat power. The input power to the heater was controlled by a DC power supply (Hewlett Packard E3632A). To measure the temperatures of the heat sink, thermocouples TC1-TC3 were glued to the heat sink using thermal epoxy (Figure 4b). TC1 was embedded in the center of the base plate, where the maximum heat sink temperature was estimated to be. TC2 and TC3 were located on the periphery of the base plate.

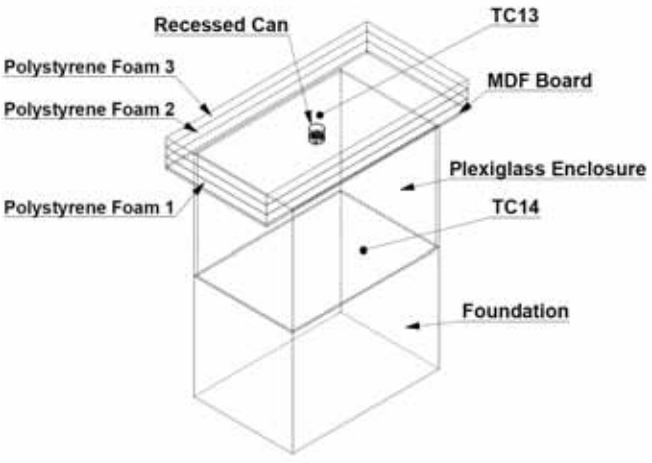

Fig. 2. Schematic of the experimental setup

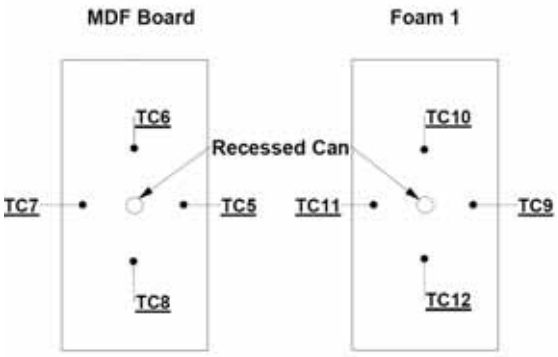

Fig. 3. Thermocouple locations of TC5-TC12

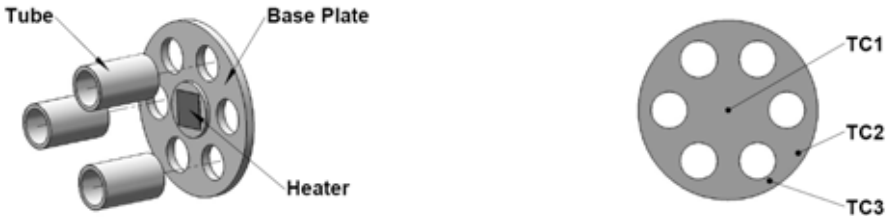

(a) (b)

Fig. 4. (a) Exploded view of heat sink (b) Thermocouple locations (TC1-TC3) on the back of the heat sink

All temperature data from the thermocouples were collected by a Data Acquisition Unit (Agilent 34970A). A custom LabVIEW program was written to control data collection. The program started collecting temperature data when all thermocouple readings differed within 1°C and terminated when steady state was reached (i.e., the changes of all thermocouple readings within five minutes are less than 0.1°C). Ambient temperature was controlled at 20 ± 1°C

In order to study the effect of radiation heat transfer, an additional setup was used to measure the emissivity of three surface conditions involved in this study: a bare aluminum surface, a painted (white high temperature spray paint) aluminum surface, and aluminum foil (Nashua Tape). The surface conditions were created on a 1.5 in. × 1.5 in. × 0.0625 in. (38.1 mm × 38.1 mm × 1.6 mm) aluminum piece, which had a 1 in. × 1 in. (25.4 mm × 25.4 mm) square resistive heater attached to its back and two T-type thermocouples embedded. When the piece was heated up and the temperature reached steady state, a pyrometer (Minolta/Land Cyclops Mini Laser) was used to measure the surface temperature. The emissivity was determined by matching the pyrometer reading to the average of the thermocouple readings. The measured emissivity was 0.15 for the bare aluminum surface, 0.91 for the white painted aluminum surface, and 0.15 for the aluminum foil. These values were used as inputs in numerical simulation to calculate heat transfer due to radiation.

4. NUMERICAL SIMULATION

Numerical simulation was conducted using finite-volume-based commercial CFD software FLUENT 6.3 to analyze the contributions of conduction, convection, and radiation for each heat sink design. As a result of the nature of the problem, a 3D steady-state solver for laminar flow was used. SIMPLE algorithm was chosen to deal with pressure-velocity coupling. Body-force-weighted scheme was used to interpolate pressure, and second-order upwind scheme to interpolate velocity and temperature.[14] For natural convection, Boussinesq approximation was applied to model temperature-dependent density.[14] For radiation, a surface-to-surface radiation model was applied. Temperature measurements TC4-TC14 on the setup were applied on the boundaries of the solid region of the numerical models, and velocity was set to be zero on the boundaries of the fluid region. To test the dependence of the numerical solution on grid size, a grid independence study was carried out by solution-based grid adaption. The initial grid contained about 600,000 cells. After adapting the initial grid to temperature gradient, the grid size increased by 10%. However, heat sink temperature changed less than 0.1%. Therefore, the initial mesh was considered to be adequate to provide precise solutions. The iterative solving process terminated when the convergence criteria were satisfied (i.e., residuals$<10^{-6}$). The numerical code was validated by comparing numerical results to experimental results on T_{hs} . Figure 5 shows the experimental and numerical (simulation) results of the maximum heat sink temperature as a function of tube length at both 3 W and 6 W. The numerical and experimental results agree very well, which validates the numerical model.

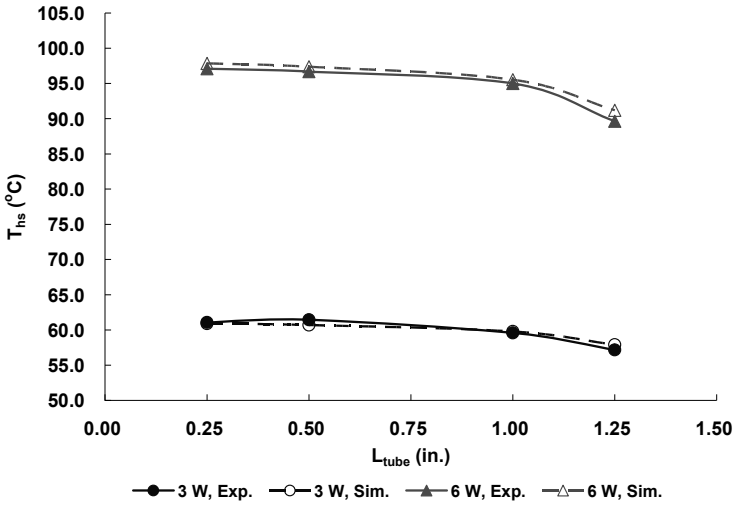

Fig. 5. Numerical results vs. experimental results

5. RESULTS

Final results are shown and discussed in this section. The base case was selected at a recessed distance of 1 in. (25.4 mm). At a heater input power of 6 W, the simulated heat sink temperature at this recessed distance was 99.2°C. In this study, pin fin, tube, and trim were investigated to understand their effect on reducing heat sink temperature in the recessed downlight application. In addition, surface emissivity was varied to show the influence on heat sink temperature.

5.1 Pin fin and tube

Figure 6 shows heat sinks with three vertical pin fins on the back, three vertical pin fins on the front, and three tubes on the front. The pin fins (0.6 in. [15.2 mm] length, 0.625 in. [15.9 mm] diameter) and the tubes (0.6 in. [15.2 mm] length, 0.625 in. [15.9 mm] outer diameter, 0.5 in. [12.7 mm] inner diameter) increased the heat sink surface area by 56% and 58%, respectively. Figure 7a shows the simulated heat sink temperatures together with that of the base case. The pin fins on the back of the heat sink did not help reduce heat sink temperature, primarily because air movement surrounding the fins was severely confined by the insulated recessed can, which resulted in little heat transfer from the fins. The pin fins on the front led to a 1°C lower heat sink temperature due to relatively better air circulation. The tubes on the front led to a 1°C lower heat sink temperature than the pin fins on the front because of increased surface area on the inner side of the tubes. Figure 7b shows the individual thermal resistances. For the pin fins on the back, the thermal resistances are almost the same as those of the base case, and large $R_{conv,hs-f}$ indicates almost no convection heat transfer from the front of the heat sink. For the pin fins on the front, $R_{conv,hs-f}$ and $R_{rad,hs-f}$ are lower due to additional convection and radiation heat transfer from the fins; $R_{conv,can}$ and $R_{rad,can}$ are slightly higher because lower can temperature weakens natural convection and radiation. Comparing the tubes and fins on the front, their individual thermal resistances are almost the same except the tubes led to lower $R_{conv,hs-f}$, which is explained by the increased surface area on the inner side of the tubes.

(a) (b) (c)

Fig. 6. (a) Pin fins on the back (b) Pin fins on the front (base plate shown in wire frame to show the fins) (c) Tubes on the front

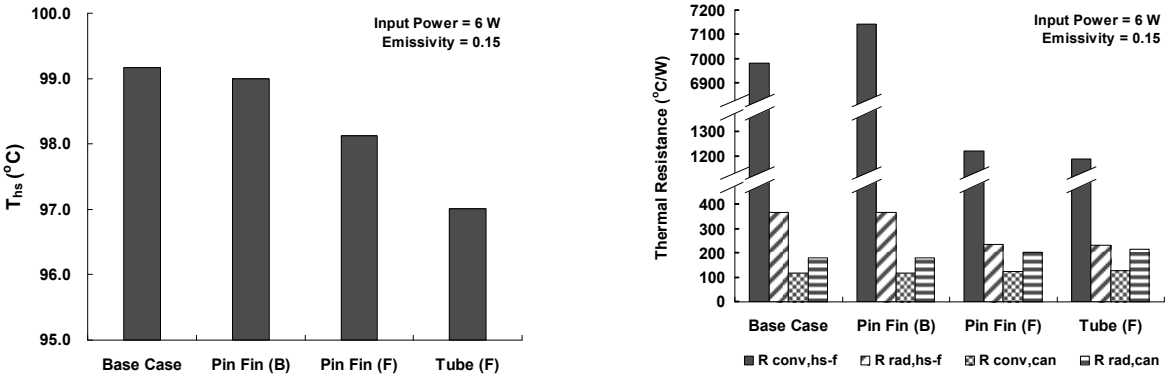

(a) (b)

Fig. 7. (a) Heat sink temperature variation of pin fins and tubes at 6 W and surface emissivity of 0.15 (b) corresponding individual thermal resistances

Figure 8 shows heat sink temperatures as a function of tube or fin length at 6 W. Both curves show the same trend and tubes led to a slightly lower temperature than fins. For the tubes, the heat sink temperature continuously decreases with increasing tube length. From 0.25 in. (6.4 mm) to 1 in. (25.4 mm), the maximum heat sink temperature decreased by 2.3°C. However, from 1 in. (25.4 mm) to 1.25 in. (31.8 mm), a significant decrease of 4.3°C was observed. The reason for decreasing temperature with increasing tube length is that the air surrounding the short tubes is stagnant and at nearly the same temperature as the tubes, while the tubes longer than 1 in. (25.4 mm) extend below the ceiling and reach the area where the air temperature is much lower. Figures 9a and 9b show individual thermal resistances for fins and tubes at four different lengths. Large $R_{conv,hs-f}$ for the pin fins and tubes at 0.25 in. (6.35 mm.) indicates almost no convection heat transfer from the front of the heat sink. $R_{conv,hs-f}$ decreases significantly as tube length increases due to decreasing surrounding air temperature, as just explained, and $R_{rad,hs-f}$ decreases because long tubes have increased view factor to the ambient. $R_{conv,can}$ and $R_{rad,can}$ remain the same for short tubes and increase for long tubes because of a lower can temperature. From the results, a further decrease in heat sink temperature can be expected by increasing the tube length. However, the scattered tubes make optical design difficult and excessive protrusion below the ceiling may affect the appearance of the fixture. Therefore, it may not be a practical solution for a recessed downlight fixture.

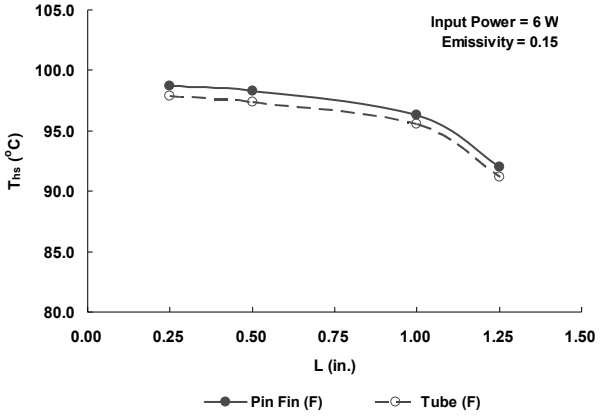

Fig. 8. Heat sink temperature variation of frontal pin fins and frontal tubes with length at 6 W and surface emissivity of 0.15

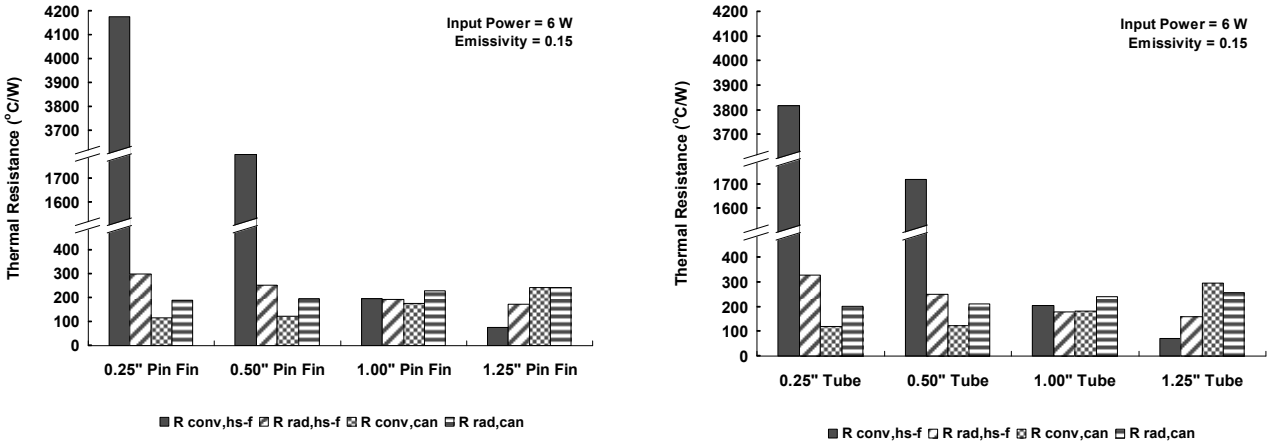

(a) (b)

Fig. 9. Individual thermal resistances of pin fins (a) and tubes (b) at 6 W and surface emissivity of 0.15

Figure 10 shows the effect of surface emissivity on reducing heat sink temperature for the 1 in. (25.4 mm) tube by increasing the surface emissivity of the front of the heat sink and tubes to 0.91 (i.e., painted aluminum surface). Figure 10a shows that increasing the surface emissivity to 0.91 results in a 8°C lower heat sink temperature. Figure 10b shows a significant decrease in $R_{rad,hs-f}$ due to the increase of surface emissivity. $R_{rad,can}$ also increases because of decreased heat sink temperature. The results indicate that a remarkable heat sink temperature can be achieved by increasing surface emissivity under natural convective conditions, confirming the important contribution of radiation heat transfer.

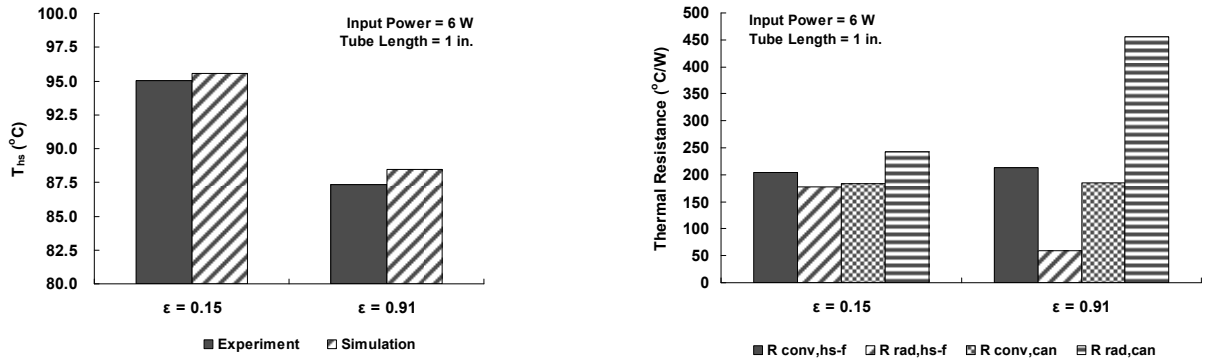

(a) (b)

Fig. 10. (a) Heat sink temperature variation with surface emissivity for 1 in. (25.4 mm) tube at 6 W (b) corresponding individual thermal resistances

5.2 Metal Trim Below the Ceiling

Figure 11 shows a heat sink design with a thin round trim (1 in. [25.4 mm] width, 0.125 in. [3.2 mm] thickness) attached to the heat sink by a straight aluminum tube (0.125 in. [3.2 mm] thick). The effect of the trim on heat sink temperature was studied by simulating four configurations, as shown in Figure 12. Case A and Case B have the straight tube only, while Case C and Case D both have the trim; Case A and Case C have surface emissivity of 0.15, while Case B and Case D have surface emissivity of 0.91. Figure 13a shows that the simulated heat sink temperatures of the four configurations systematically decreased due to the addition of trim and increased surface emissivity. As a result, a significant decrease of 38.2°C (as compared to the base case) was achieved in Case D. The significant decrease in heat sink temperature due to the addition of trim and increased emissivity can be justified by individual thermal resistances, as shown in Figure 13b ($R_{conv,can}$ and $R_{rad,can}$ are not available because they do not exist in the current configurations). The addition of trim significantly reduces $R_{conv,hs-f}$, as shown by comparing Case A and Case C or Case B and Case D, because the air flow surrounding the trim circulates freely and the air temperature is lower. Increasing surface emissivity significantly reduces $R_{rad,hs-f}$ (comparing Case A and Case B or Case C and Case D).

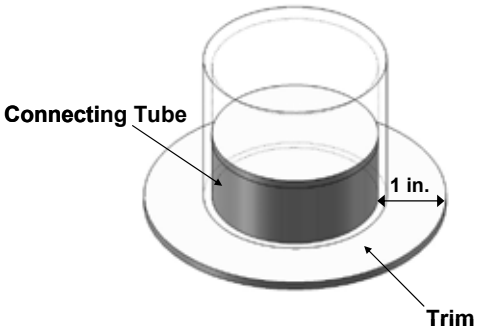

Fig. 11. Heatsink with a 1 in. (25.4 mm) trim

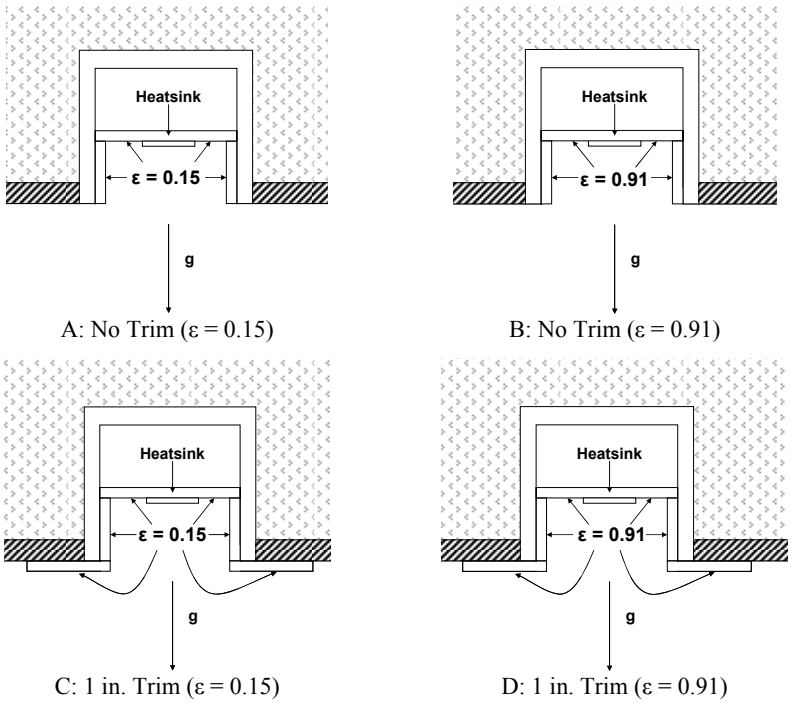

Fig. 12. Four configurations

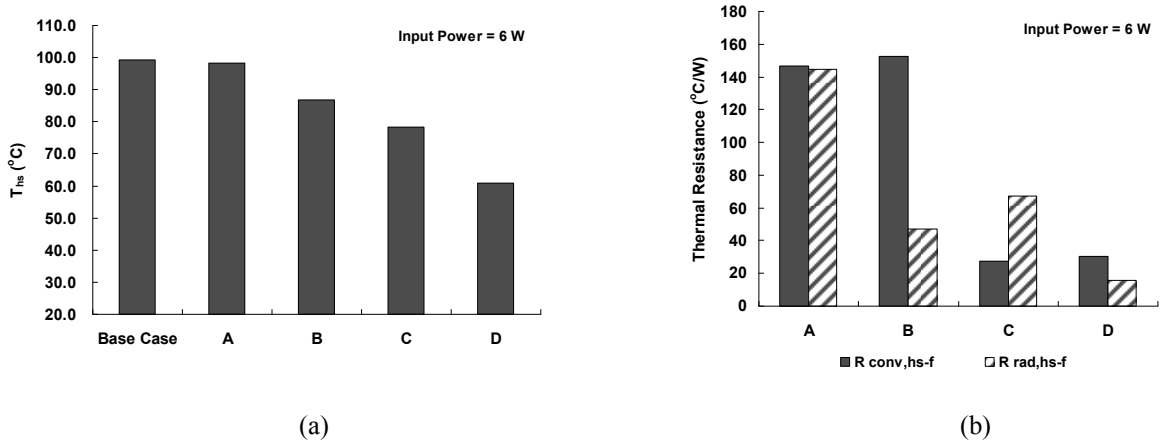

(a) (b)

Fig. 13. (a) Heat sink temperature variation of the four cases at 6 W (b) corresponding individual thermal resistances

6. DISCUSSION

The experimental investigation and numerical simulation on the 2.5 in. (63.5 mm) recessed downlight fixture indicated that heat sink temperature could be significantly reduced by adding trim with high surface emissivity. With this knowledge, a 4 in. (101.6 mm) recessed downlight fixture with a trim of 2 in. (50.8 mm) width and 0.25 in. [6.4 mm] thickness was designed and prototyped. The fixture was made in a three-piece assembly and held together by set screws, and all joint surfaces were filled with thermal grease (Wakefield Engineering 126) to reduce thermal interface resistance. The fixture was tested in the same setup, as described in the section 3, before and after being painted. The ambient temperature was controlled at 22 ± 1°C. Figure 14 shows experimental and numerical results at input powers of 9 W, 12

W, and 15 W. As expected, higher emissivity resulted in much lower heat sink temperature at the three input powers. The fixture had a heat sink temperature of less than 70°C up to 14 W, 15°C lower than the bare trim. Figure 15 shows heat sink temperature variation with trim width. The heat sink temperature decreases as the trim width increases, but the rate of change decreases with the trim width because the trim's conduction thermal resistance increases and the temperature distribution over the trim surface becomes less uniform. Figure 16 shows the impact of contact thermal resistance at the joint surfaces. It is clear that by making the fixture in one piece (or removing the contact thermal resistance), heat sink temperature can decrease by 5.7°C (9 W) to 9.6°C (15 W).

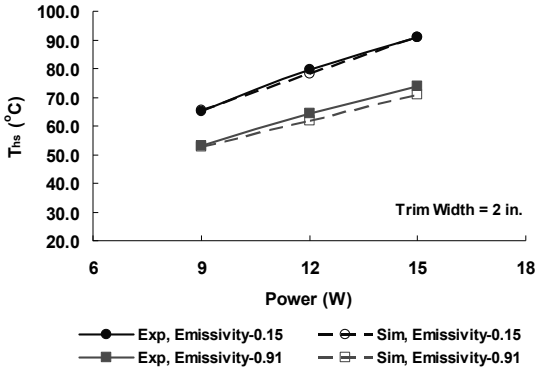

Fig. 14. Experimental and numerical results of a 4 in. (101.6 mm) LED recessed downlight fixture

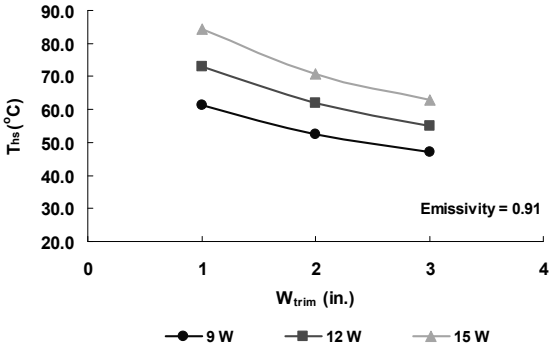

Fig. 15. Effect of trim width

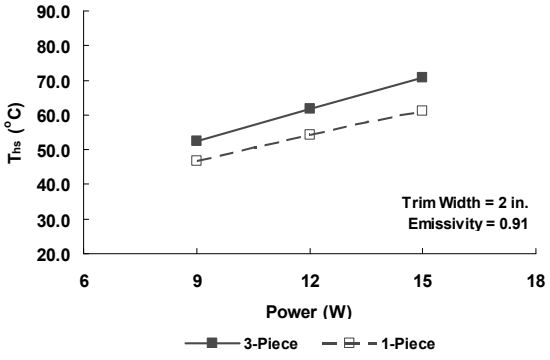

Fig. 16. Effect of contact thermal resistance

7. SUMMARY

In this paper, thermal solutions for a recessed LED downlight fixture were investigated so that LED junction temperature remained reasonable during operation. Experiments and simulations were conducted to understand the contribution of heat transfer mechanisms to heat sink temperature. From the investigation of a 2.5 in. (63.5 mm) recessed fixture model, it was concluded that an extended trim with high surface emissivity could significantly reduce the heat sink temperature of a recessed downlight. A 4 in. (101.6 mm) recessed downlight fixture was then designed and tested, and results confirmed the feasibility of the design for recessed downlight application.

ACKNOWLEDGMENTS

The authors thank Jean Paul Freyssinier, Nick Skinner, Martin Overington, and Howard Ohlhous of the Lighting Research Center for their support in the experiment setup. Jennifer Taylor of the Lighting Research Center is also thanked for her valuable help in preparing this manuscript.

REFERENCES

[1] Narendran, N. and Y. Gu. 2005. Life of LED-based white light sources. IEEE/OSA Journal of Display Technology 1(1): 167–171.

[2] Narendran, N., Y. Gu, J.P. Freyssinier, H. Yu, and L. Deng. 2004. Solid-state lighting: Failure analysis of white LEDs. Journal of Crystal Growth 268(3-4): 449–456.

[3] Gu, Y., N. Narendran, and J.P. Freyssinier. 2004. White LED performance. Fourth International Conference on Solid State Lighting, Proceedings of SPIE 5530: 119-124.

[4] Christensen, A., M. Ha, and S. Graham. 2007. Thermal management methods for compact high power LED arrays. Seventh International Conference on Solid State Lighting, Proceedings of SPIE 6669: 66690Z.

[5] Sheu, G. J., F. S. Hwu, S. H. Tu, W. T. Chen, J. Y. Chang, and J. C. Chen. 2005. The heat dissipation performance of LED applied a MHP. Fifth International Conference on Solid State Lighting, Proceedings of SPIE 5941: 594113.

[6] Shin, M. W. 2006. Thermal design of high-power LED package and system. Sixth International Conference on Solid State Lighting, Proceedings of SPIE 6355: 635509.

[7] Jang, S. H., and Shin, M. W. 2008. Thermal analysis of LED arrays for automotive headlamp with a novel cooling system. IEEE Transactions on Device and Materials Reliability 8(3): 561–564.

[8] Bar-Cohen, A., M. Iyengar, and A.D. Kraus. 2003. Design of optimum plate-fin natural convective heat sinks. Journal of Electronic Packaging 125(2): 208–216.

[9] Huang, R.T., W.J. Sheu, H.Y. Li, C.C. Wang, K.S. Yang. 2006. Natural convection heat transfer from square pin fin heat sinks subject to the influence of orientation. 22nd IEEE SEMI-THERM Symposium, pp.102–105.

[10] Concepcion, J. 2004. Master's Thesis: Passive Heatsinking for Recessed Luminaires. Lighting Research Center, Rensselaer Polytechnic Institute.

[11] Feenstra. 1998. U.S. Patent 5,781,411, Heat Sink Utilizing the Chimney Effect.

[12] Rao, V.R. and S.P. Venkateshan. 1996. Experimental study of free convection and radiation in horizontal fin arrays. International Journal of Heat and Mass Transfer 39(4): 779–789.

[13] Rao, V. D., S. V. Naidu, B. G. Rao, K. V. Sharma. 2006. Heat transfer from a horizontal fin array by natural convection and radiation – a conjugate analysis. International Journal of Heat and Mass Transfer 49: 3379–3391.

[14] Fluent Inc. Fluent 6.3 User's Guide.